Journal of Materials Chemistry A

Accepted Manuscript

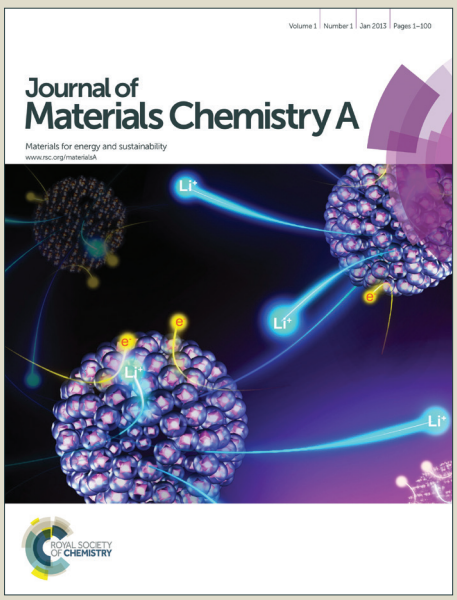

ROYAL SOCIETY OF CHEMISTRY

www.rsc.org/materialsA

PAPER www.rsc.org/materials | Journal of Material Chemistry A

In-situ growth of monodisperse Fe_3O_4 nanoparticles on graphene as flexible paper for supercapacitor

Miaomiao Liu, Jing Sun *

Received (in XXX, XXX) Xth XXXXXXXXX 200X, Accepted Xth XXXXXXXXX 200X
First published on the web Xth XXXXXXXXX 200X
DOI: 10.1039/b000000x

A well-organized Fe_3O_4/ graphene sheet composite (GS/Fe_3O_4) paper has been constructed via a universal three-step method. Firstly, graphene oxide/Fe_2O_3 composite (GO/Fe_2O_3) dispersion is prepared, and it subsequently followed by a vacuum filtration of the dispersion to obtain GO/Fe_2O_3 composite paper, with heat treatment of GO/Fe_2O_3 paper to finally achieve GS/Fe_3O_4 paper. Fe_3O_4 nanoparticles of ~5 nm are in situ grown and anchored on graphene sheets uniformly by covalent chemical bonding. The three-dimensional (3-D) conductive paper provides good electrical contact and improves the dispersion of the well-adhered Fe_3O_4 nanoparticles, further boosting the accessible capacity. As a consequence, GS/Fe_3O_4 paper exhibits excellent rate performance and cyclic stability as a flexible anode material for supercapacitors. The optimized GS/Fe_3O_4 paper could achieve a high specific capacitance of 368 F g^{-1} at 1 A g^{-1} and remain 245 F g^{-1} at 5 A g^{-1} after 1000 cycles, suggesting a promising application to fabricate flexible energy storage devices. This work opens up a new insight into the design of GS/metal oxide paper as a flexible electrode.

1. Introduction

Up to now, a global attention has been paid on various energy-storage devices, such as Li-ion batteries, fuel cells, supercapacitors and so on, due to the ever-increasing energy demand and environmental problems.[1-5] Among them, supercapacitors have shown highly promising application because of their high power density, low cost, and long cycle life.[6-7] According to the energy storage mechanisms, supercapacitors could be divided into two types.[8] The first one is electrical double layer capacitor (EDLC), which involves a non-Faradic process.[9] The other is pseudocapacitor, which bears a Faradic redox reaction for energy storage.[10-11] The specific capacitance of pseudocapacitor is much higher than that of EDLC on account of the Faradic redox reaction on the surface of pseudocapacitive materials. Therefore, pseudocapacitive materials, such as NiO,[12] $Ni(OH)_2$,[13] $NiCo_2O_4$,[14] Co_3O_4[15] and MnO_2,[16] which show high specific capacitance, have been investigated widely. The researches being committed to the above positive electrode materials (working potential above 0 V vs. Hg/HgO) have made great achievements. However, only a few reports on the study of negative electrode materials (working potential below 0 V) owing to their unsatisfying specific capacitance. It is especially important to explore the ideal anode materials which can match with the cathode materials well. Fe_3O_4, with the working potential up to –1 V vs. Hg/HgO, has the advantage of easy redox reaction, non-toxicity and low cost. Thus Fe_3O_4 is considered as one of the most prospective negative electrode materials. Nevertheless, its poor electrical conductivity leads to slower electron transport rate and less active material availability. The disadvantage causes its poor capacitance of 60-100 F g^{-1}.[17-19] Incorporating conductive materials, such as active carbon,[17] carbon nanotubes[20-21] and graphene,[18, 22-24] with Fe_3O_4 to generate composites is a great way to solve the problem of low electrical conductivity. Of all the conductive materials, graphene represents huge superiority due to its large surface area (2630 m^2 g^{-1}), great conductivity, and mass production. In addition, the synergistic effects by combining Fe_3O_4 with graphene could improve their electrochemical performance extremely.

Nowadays, only a few studies have been focused on the graphene/Fe_3O_4 composites as anode materials for supercapacitors. For example, Qu et al.[22] prepared 2D sandwich-like sheets of Fe_3O_4 grown on graphene as high energy anode material and achieved a specific capacitance of 326 F g^{-1} at 0.5 A g^{-1}. Wang and coworkers[24] reported a hydrothermal method to synthesize graphene/Fe_3O_4 composites, delivering a capacitance of 220 F g^{-1} at 0.5 A g^{-1} after 3000 cycles. However, the working electrodes in the previous reports were prepared by the traditional slurry-coating technology. The electrodes were fabricated by binder and conductive carbon. In fact, the binder will decrease the conductivity of electrode and restrain electron transport, further leading to the poor electrochemical performance. Moreover, the conductive carbon hardly contributes to capacitance, while it occupies a certain volume of electrode. The above reasons hinder the potential application of graphene/Fe_3O_4 composites in high performance supercapacitors. Therefore, it is highly desirable to design a novel, flexible and binder-free electrode to obtain the ideal electrochemical performance.

In this work, a well-organized flexible GS/Fe_3O_4 paper has been built. Graphene forms a three dimensional conductive network, with Fe_3O_4 nanoparticles of ~5 nm being distributed homogeneously. Fe_3O_4 nanoparticles are in situ grown and anchored on graphene sheets by covalent chemical bonding. GS

The State Key Lab of High Performance Ceramics and Superfine Microstructure, Shanghai Institute of Ceramics, Chinese Academy of Sciences, 1295 Dingxi Road, Shanghai 200050, P.R. China. Fax: +86-21-52413122; Tel: +86-21-52414301;

E-mail: jingsun@mail.sic.ac.cn

† Electronic Supplementary Information (ESI) available. See DOI: 10.1039/b000000x/

as a flexible confinement material to support Fe_3O_4 nanoparticles prevents the agglomeration of nanoparticles and offers facile electron transport pathway. Meanwhile, Fe_3O_4 nanoparticles separate GS to avert their restacking, further to increase interlayer porosity of the paper. Benefiting from the unique 3-D architecture, the flexible GS/Fe_3O_4 paper exhibits excellent rate performance and cyclic stability compared to the traditional electrodes. The optimized GS/Fe_3O_4 paper could achieve a high specific capacitance of 368 F g^{-1} at 1 A g^{-1}, indicating a promising application as a flexible negative electrode. The flexible free-standing paper is expected to play a vital part in fabricating flexible energy-storage devices.

2. Experimental procedure

2.1 Materials preparation

Graphene oxide (GO) was prepared by a modified Hummers method.[25] Then, certain content of $Fe(NO_3)_3$•$9H_2O$ was dissolved in 35 mL of DMF, to which 8 mL of 5 mg mL^{-1} GO suspension was added. The dispersion was kept stiring at 90 °C for 1 h. GO/Fe_2O_3 composite paper was obtained by vacuum filtrating the resulting dispersion through a Millipore membrane filter (47 mm in diameter, 0.22 mm in pore size), followed by vaccum drying and peeling off. Finally, thermal reduction of GO/Fe_2O_3 composite paper to GS/Fe_3O_4 composite paper was accomplished at 550 °C for 2 h in Ar (Scheme 1). To attain the optimal electrochemical performance, the different weight ratio of Fe_3O_4 in GS/Fe_3O_4 was explored. The precursors and obtained products were denoted as GO/Fe_2O_3-1, GO/Fe_2O_3-2, GO/Fe_2O_3-3 and GS/Fe_3O_4-1, GS/Fe_3O_4-2, GS/Fe_3O_4-3, respectively. The corresponding Fe_3O_4 contents in the GS/Fe_3O_4 composites are 48.4%, 59.6% and 64.8%. In comparison, pure Fe_3O_4 was prepared by reducing Fe_2O_3 at 350 °C for 1 h in Ar/H_2 (95:5).

2.2 Materials characterization

The structures of the products were examined by X-ray power diffraction (XRD) on Rigaku D/Max-2550V diffractometer using Cu Kα radiation. The morphology of the products was observed on a transmission electron microscope (TEM Tecnai G20 FEI 200KV) and a scanning electron microscope (SEM JEOL S-4800). Raman spectroscopy was conducted on a DXR Raman Microscope with a 532 nm excitation length. Thermal gravimetric analysis (TGA) was carried out in air at a heating rate of 10 °C min^{-1}. The specific surface area was measured by Brunauer-Emmett-Teller (BET) method at 77 K in N_2 atmosphere using Micromeritics ASAP 2010 surface area analyzer. The conductivity of GS/Fe_3O_4 composite papers was tested by means of Accent HL 5500 at room temperature.

2.3 Electrochemical Measurements

GS/Fe_3O_4 composite papers were directly used as working electrodes without any binder and additive. The GS/Fe_3O_4-3 and Fe_3O_4 traditional electrodes, named trad. electrodes, were prepared by a slurry-coating technology. Typically, the samples were mixing with acetylene black and polytetrafluoroethylene (PTFE) binder (weight ratio of 8:1:1) in N-methylpyrrolidone (NMP) to form slurries. After being stirred uniformly, the slurries were pasted onto carbon current collector and dried under vacuum at 100 °C for 12 h. All electrochemical measurements were performed in a three-electrode system. The working electrode was dipped in 1 M KOH aqueous solution. A platinum wire and a Hg/HgO were used as counter electrode and reference electrode, respectively. Cyclic voltammetrys (CV) measurments were carried out on a Parstat 2273 electrochemical station (Princeton applied research CO., Ltd, USA). Galvanostatic charge/discharge tests were performed on a LAND CT2001A cell 50 measurement system.

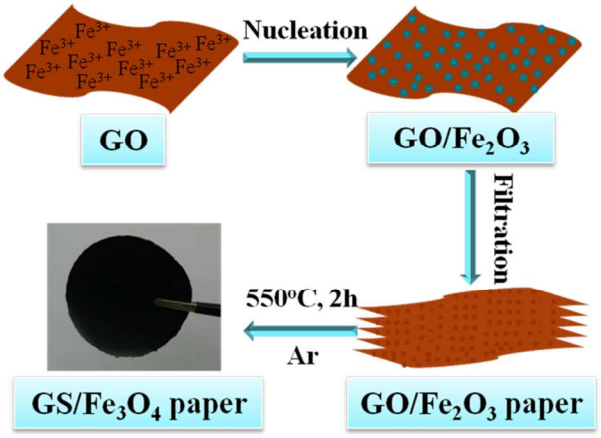

Scheme 1 A schematic illustration of the fabrication processes of GS/Fe_3O_4 composite paper.

3. Results and discussion

The preparation process for GS/Fe_3O_4 composite paper is illustrated in Scheme 1. Firstly, Fe_2O_3 nanoparticles are in situ grown and anchored on the surface of GO by covalent chemical bonding. In order to optimize the GS/Fe_3O_4 composite paper, the precursors (GO/Fe_2O_3) with various iron oxide contents were studied. Fig. 1 shows TEM images of the

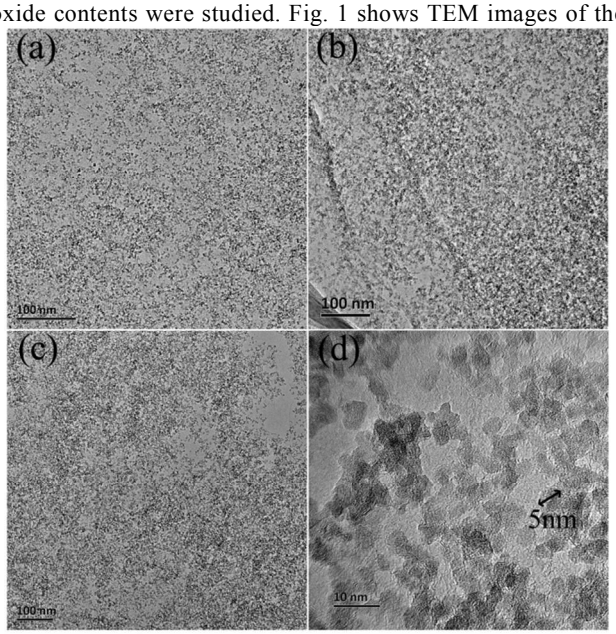

Fig. 1 TEM images of (a) GO/Fe_2O_3-1, (b) GO/Fe_2O_3-2, (c) GO/Fe_2O_3-3, (d) HRTEM image of GO/Fe_2O_3-3.

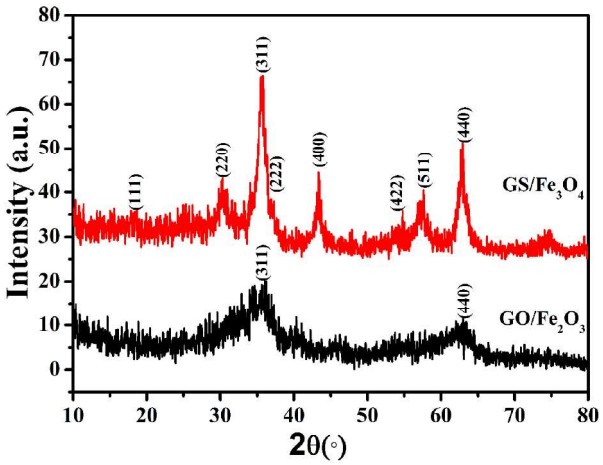

Fig. 2 XRD patterns of GO/Fe_2O_3 and GS/Fe_3O_4 composites.

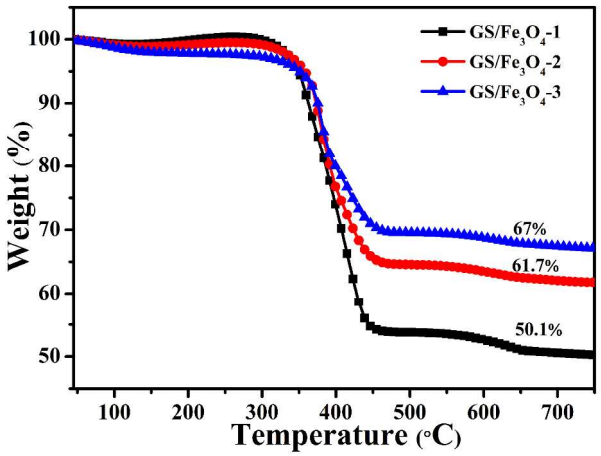

Fig. 3 TG profiles of GS/Fe_3O_4 composites with different weight ratio.

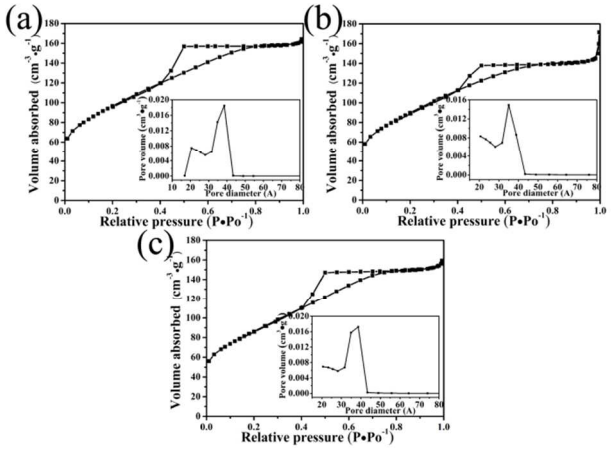

Fig. 4 Nitrogen adsorption-desorption isotherms (with the BJH pore size distributions plots in the insets.) measured at 77K for the (a) GS/Fe_3O_4-1, (b) GS/Fe_3O_4-2, (b) GS/Fe_3O_4-3.

GO/Fe_2O_3 composites with different weight ratio. Fe_2O_3 nanoparticles of ~5nm are homogeniously distributed on the GO sheets. However, the pure Fe_2O_3 particles without GO present agglomerated blocky-shaped structure with irregular larger size (Fig. S1). It can be noted that, the adding of GO decreases the size and improves the uniformity of Fe_2O_3 nanoparticles. This is ascribed to the dispersing nucleation of Fe^{3+} assisted by the oxygen groups of GO. Moreover, with the content of iron source increasing, Fe_2O_3 nanoparticles on the surface of GO turn dense, indicating the increment of Fe_2O_3 content in GO/Fe_2O_3 composites. After vacumm filtration, flexible GO/Fe_2O_3 composite papers are obtained. Finally, the GO/Fe_2O_3 papers are transformed into GS/Fe_3O_4 papers by a simple thermal reduction. Fig. 2 displays XRD patterns of GO/Fe_2O_3 and GS/Fe_3O_4 composites. The diffraction peaks of GO/Fe_2O_3 can be assigned to maghemite-c (λ-Fe_2O_3-JCPDS no. 39-1346). After heat treatment, Fe_2O_3 are successfully reduced to Fe_3O_4. All the diffraction peaks are well indexed to magnetite (Fe_3O_4-JCPDS no. 19-0629), proving that GS/Fe_3O_4 composite have no other impurity phases. To certify the reduction of GO, the Raman spectroscopy (Fig. S2) of GO/Fe_2O_3 and GS/Fe_3O_4 composites was detected. The Raman spectra reveals the increasing ratio of D band (~1335 cm^{-1}) to G band (~1589 cm^{-1}) from 1.42 to 1.77. This manifests the reduction of GO, in good agreement with the previous reports.[26-27] The above conclusion reveals that GS/Fe_3O_4 composite is successfully achieved by reducing GO/Fe_2O_3 composite.

Thermogravimetric analysis (TGA) was performed to determine Fe_3O_4 contents in the GS/Fe_3O_4 composite papers precisely. The resulting product is only Fe_2O_3 after TGA, and the corresponding Fe_2O_3 content is 50.1%, 61.7% and 67% for GS/Fe_3O_4-1, GS/Fe_3O_4-2 and GS/Fe_3O_4-3. Based on the TGA results (Fig. 3), the Fe_3O_4 contents in GS/Fe_3O_4 composites are calculated to be 48.4%, 59.6% and 64.8% respectively. The iron oxide content increases gradually, which is consistent with the result of TEM. The weight ratio of GS and Fe_3O_4 would influences specific surface area of the composite. Fig. 4 represents the Nitrogen adsorption/desorption isotherms of GS/Fe_3O_4 composites with different weight ratio. The specific surface areas are 346.1, 323.1 and 310 m^2 g^{-1} for GS/Fe_3O_4-1, GS/Fe_3O_4-2 and GS/Fe_3O_4-3, respectively. Hence, with the reduction of graphene content, the specific surface area of GS/Fe_3O_4 composite decreases. It is reasonable because GS with larger specific surface area could provide more surface area in the composites.[28-30] Besides, the GS/Fe_3O_4 composites in this work possess much larger specific surface area than that reported previously.[29-32] Furthermore, the GS/Fe_3O_4 composites exhibit type IV nitrogen adsorption and desorption isotherms, declaring the presence of mesopores. Specifically, the pore sizes are 3-4 nm calculated by the BJH method from the pore size distribution plots. As well known, the large specific surface area and suitable pore size distribution in the range of 2-5 nm is favorable for electrochemical reaction.[33-34] Because the large specific surface areas can provide the high availability of electrode materials. Meanwhile, the appropriate pore size facilitates better diffusion and accession of electrolyte ions through pore channels for efficient redox reactions during the charge storage process. From this point, the GS/Fe_3O_4 composite papers could be used as excellent negative electrode materials.

To characterize the composite paper in detail, TEM and SEM of GS/Fe_3O_4-3 paper were further investigated. From the top-view images (Fig. 5a), the Fe_3O_4 nanoparticles are uniformly anchored on the surface of GS without any

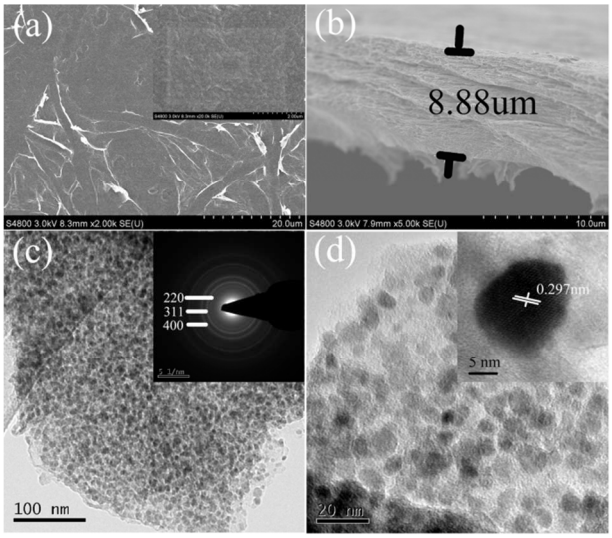

Fig. 5 (a) Top-view SEM images of GS/Fe_3O_4-3 composite paper. (b) Cross-section SEM image of GS/Fe_3O_4-3 composite paper. (c) TEM image of GS/Fe_3O_4-3 composite. (d) HRTEM images of GS/Fe_3O_4-3 composite.

aggregates. The cross-section image discloses 3-D layer structure of GS/Fe_3O_4-3 paper with the thicknesss of ~8.88 μm (Fig. 5b). To further observe the inner morphology, TEM images are given in Fig. 5c-d. Fe_3O_4 nanoparticles of ~5nm are dispersed on the surface of GS homogeneously. The inset of Fig. 5c shows the selected-area electron diffraction (SAED) pattern. The rings index to the (220), (311), and (400) planes of Fe_3O_4, in accordance with the XRD data. The HRTEM image (Fig. 5d) reveals the lattice distance of 0.297 nm, corresponding to the (220) plane of Fe_3O_4. In the 3-D layer structure, GS improves the dispersion of Fe_3O_4 nanoparticles, while Fe_3O_4 prevents the agglomeration of GS. In consequence, the unique structure facilitates electron transport, further boosting the accessible capacity of GS/Fe_3O_4-3 paper electrode.

To confirm the best mass ratio of GS/Fe_3O_4 papers as negative electrodes, the electrochemical performance of GS/Fe_3O_4 papers with different Fe_3O_4 contents was evaluated by cyclic voltammetry and galvanostatic charge/discharge. The CV measurments of GS/Fe_3O_4 composite papers (Fig. 6a) are recorded at 5 mV s^{-1} in the potential range of -1-0 V. The width of the CV curves decreases in the order of GS/Fe_3O_4-3>GS/Fe_3O_4-2>GS/Fe_3O_4-1, demonstrating the reduction of specific capacitance in sequence. To discuss in detail, galvanostatic charge/discharge measurements of GS/Fe_3O_4 composite papers are carried out at various current densities in a potential window of -1-0 V. The specific capacitance is calculated from the corresponding galvanostatic discharge curves (Fig. 6b-d) according to the following equation:

$$C_s = \frac{I\Delta t}{m\Delta v}$$

where C_s is the specific capacitance, I stands for the current density, m represents the mass of active materials in the electrode, △V is the voltage difference. As determined in Fig. 6e, GS/Fe_3O_4-3 paper discloses much better capacitance performance compared with others at all current densities. The

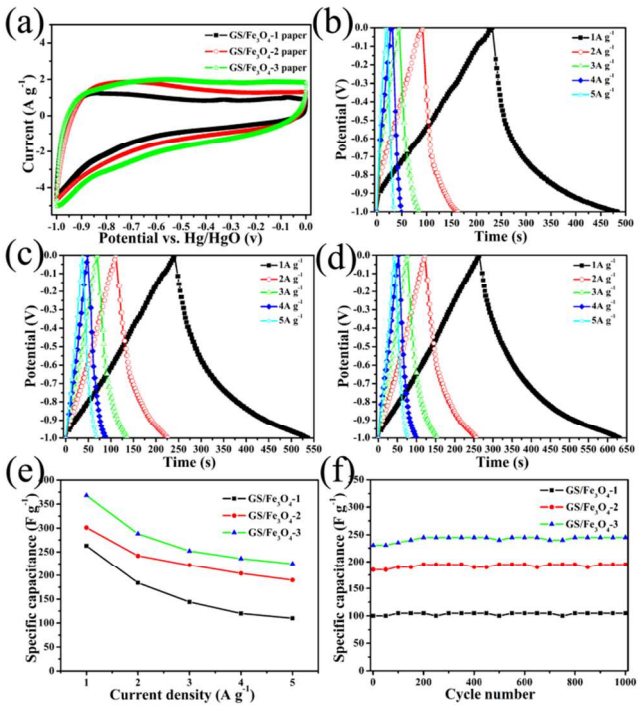

Fig. 6 Electrochemical characterizations of GS/Fe_3O_4 composites papers: (a) CV curves at a scan rate of 5 mV s^{-1}. Galvanostatic charge–discharge curves of GS/Fe_3O_4-1 (b) GS/Fe_3O_4-2 (c) GS/Fe_3O_4-3 (d) at different current densities. (e) Average specific capacitance at different current densities. (f) Cyclic performance at 5 A g^{-1}.

Table 1. Physical property of GS/Fe_3O_4 papers

Samples	Fe_3O_4 contents	Specific surface area (m^2 g^{-1})	Resistivity (ohm $square^{-1}$)
GS/Fe_3O_4-1	48.4	346.1	14.5
GS/Fe_3O_4-2	59.6	323.1	16.9
GS/Fe_3O_4-3	64.8	310	20.2

specific capacitance of GS/Fe_3O_4-3 paper is calculated to be 368 F g^{-1} at a current density of 1 A g^{-1} based on total mass of the paper. However, the capacitance value of GS/Fe_3O_4-1 and GS/Fe_3O_4-2 papers gradually decreases to 263 and 301 F g^{-1}, both poorer than the GS/Fe_3O_4-3 paper. Besides, the GS/Fe_3O_4-3 paper possesses large specific capacitance of 225 F g^{-1} even at the high current density of 5 A g^{-1}. After the 1000-cycle test at 5 A g^{-1} (Fig. 6f), the specific capacitance of GS/Fe_3O_4-3 paper is still as high as 245 F g^{-1}, suggesting excellent cyclic performance. It is noteworthy that GS/Fe_3O_4-3 paper presents the optimized performance compared with GS/Fe_3O_4-1 and GS/Fe_3O_4-2 papers at all current densities, in consistent with the conclusion of CV testing. We can explore the reason from the physical properties why GS/Fe_3O_4-3 paper displays the best performance (Table 1). For electrode materials, the specific surface area, mass ratio of active materials, and conductivity are generally crucial for the specific capacitance. In this study, from GS/Fe_3O_4-1 to GS/Fe_3O_4-2 and GS/Fe_3O_4-3, the content of GS decreases gradually, leading to the reduction of their specific surface areas and conductivities. The two factors are unfavorable for the specific capacitance. While the mass ratio of Fe_3O_4 as active material increases gradually, which may offer more

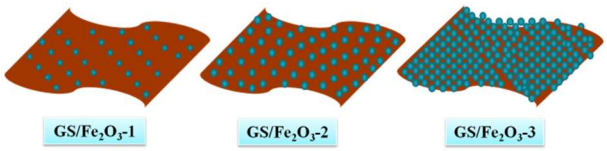

Scheme 2 A schematic illustration of GS/Fe_3O_4 composites with different Fe_3O_4 content.

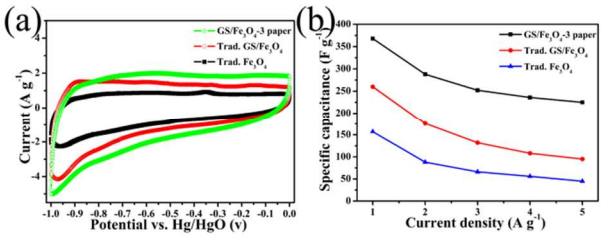

Fig. 7 (a) CV curves of GS/Fe_3O_4-3 paper, trad. GS/Fe_3O_4 and trad. Fe_3O_4 at a scan rate of 5 mV s^{-1}. (b) Average specific capacitance at different current densities.

Faradic redox reaction, further enhance the specific capacitance greatly. This is reasonable because even in the GS/Fe_3O_4-3 composite, we can see that Fe_3O_4 nanoparticles of ~5nm are monodisperse on the surface of GS from the TEM image. The Fe_3O_4 content is not much enough to cover the GS. Therefore, the contact points between graphene and Fe_3O_4 as the relative proportion of grapheme is reduced are increased, as shown in Scheme 2. Apparently, the specific surface area and conductivity of the three GS/Fe_3O_4 papers change slightly, so Fe_3O_4 content influences more significantly. Therefore, the comprehensive effect of three factors is that GS/Fe_3O_4-3 exhibits optimal electrochemical performance.

To highlight the advantage of the unique 3-D GS/Fe_3O_4-3 paper as negative electrode, the conventional electrodes of Fe_3O_4 and GS/Fe_3O_4-3 (with 10wt% acetylene black, 10wt% PTFE binder, 80wt% active material) were prepared by a slurry-coating technology, denoted as Trad. Fe_3O_4 and Trad. GS/Fe_3O_4 respectively. From the CV curves (Fig. 7a), we can easily figure out that the capacitance of GS/Fe_3O_4-3 paper is much higher than those of Trad. Fe_3O_4 and Trad. GS/Fe_3O_4. And Trad. GS/Fe_3O_4 has better performance compared to Trad. Fe_3O_4. Futhermore, the Galvanostatic charge/discharge measurements were performed to further study their electrochemical performance (Fig. S3). Fig. 7b indicates average specific capacitance calculated from the galvanostatic discharge curves at different current densities. The specific capacitance values of GS/Fe_3O_4-3 paper are 368, 288, 252, 236, and 225 F g^{-1} at 1, 2, 3, 4 and 5 A g^{-1}, respectively. For Trad. Fe_3O_4 and Trad. GS/Fe_3O_4, the values are 157, 88, 66, 56, 45 and 260, 176, 132, 108, 95 F g^{-1}. Moreover, GS/Fe_3O_4-3 paper possesses the specific capacitance of 225 Fg^{-1} at a high current density of 5 A g^{-1}, ~61.1% of that at 1 A g^{-1}. While for Trad. Fe_3O_4 and Trad. GS/Fe_3O_4, the corresponding capacitance retention is 28.7% and 36.5% respectively. In addition, the specific capacitance values stabilize at 245, 95 and 45 Fg^{-1} for GS/Fe_3O_4-3 paper, Trad. GS/Fe_3O_4 and Trad. Fe_3O_4 after 1000 cycles, respectively. Evidently, the GS/Fe_3O_4-3 paper owns the best capacitance and rate performance, followed by Trad. GS/Fe_3O_4, and Trad. Fe_3O_4 is the worst. The superior performance of GS/Fe_3O_4-3 paper can be attributed to the following reasons. (i) As a flexible confinement material to support Fe_3O_4 nanoparticles, GS prevents the agglomeration of Fe_3O_4 nanoparticles. Thus it increases their effective availability and improving the accessible capacitance. (ii) GS provides good electrical contact and paves a highway for electron transport, further boosting the rate performance and cycle stability. (iii) Fe_3O_4 nanoparticles separate GS and prevent restacking, providing better immersion and diffusion of electrolyte ions through pore channels for efficient redox reactions during the charge storage process. The three reasons explain that the introduction of GS can promote electrochemical performance, further verifying the more advantage of GS/Fe_3O_4-3 paper and Trad. GS/Fe_3O_4 than Trad. Fe_3O_4 as supercapacitor. Compared with Trad. GS/Fe_3O_4, GS/Fe_3O_4-3 paper has its own unique merits. First of all, the flexible paper acted as electrode avoids the addition of an electrically insulating polymer binder, promoting the charge transfer rate. Secondly, GS offers a continuous conductive network to decrease the particle-particle interface resistance efficiently, improving the availbility of Fe_3O_4 during redox reactions. Thirdly the interlayer spacing of paper facilitates the electrolyte ions transportion. As a result, this unique layered GS/Fe_3O_4-3 paper can dramatically improve the cycling stability and rate capability of Fe_3O_4 as an anode material for supercapacitors.

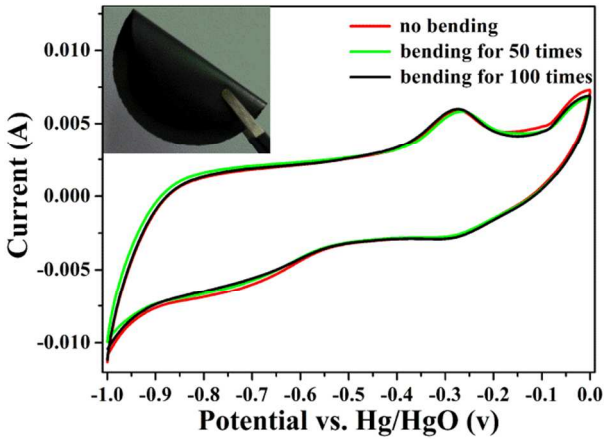

Fig. 8 The CV cycles of GS/Fe_3O_4-3 paper at different bending times (The inset is the digital photo of GS/Fe_3O_4-3 paper.).

As well known, the mechanical flexibility and bending properties of the paper electrode is significant because it is critical for device assembly. To prove the mechanical flexibility of GS/Fe_3O_4-3, the CV curves of GS/Fe_3O_4-3 paper were measured at different bending times. As shown in Fig. 8, after the paper electrode is bended for 50 and 100 times, the CV curves are almost coincided with that of no bending. There is no capacitance loss after bending, which further proves that GS/Fe_3O_4 paper is a prospective candidate as flexible supercapactor.

4. Conclusion

In summary, a three-step approach is presented for the construction of fexible GS/Fe_3O_4 composite paper. Fe_3O_4 nanoparticles of ~5 nm are uniformly in situ grown and anchored on the surface of GS by covalent chemical bonding.

The graphene sheet functions as conductive agent and binder at the same time. Rapid charge transport from the Fe_3O_4 nanoparticles to the underlying graphene provides well redox reactions. The optimized GS/Fe_3O_4 paper (64.8%) exhibits excellent rate performance and cyclic stability. It could achieve a high specific capacitance of 368 F g^{-1} at 1 A g^{-1}, and 225 F g^{-1} at 5 A g^{-1}, making GS/Fe_3O_4 paper a promising application as a flexible negative electrode material. This work opens up a universal and economic strategy to fabricate other GS/metal oxide composite papers for flexible energy-storage devices.

Acknowledgements

This work is supported by the National Basic Research Program of China (2012CB932303), the National Natural Science Foundation of China (Grant No. 51172261) and the supportion from the committee of Shanghai Science and Technology (13XD1403900).

References

1. K. Fu, O. Yildiz, H. Bhanushali, Y. X. Wang, K. Stano, L. G. Xue, X. W. Zhang and P. D. Bradford, *Adv. Mater.*, 2013, **25**, 5109-5114.
2. B. Koo, H. Xiong, M. D. Slater, V. B. Prakapenka, M. Balasubramanian, P. Podsiadlo, C. S. Johnson, T. Rajh and E. V. Shevchenko, *Nano Lett*., 2012, **12**, 2429-2435.
3. H. Chang, S. H. Joo, and C. Pak, *J. Mater. Chem.*, 2007, **17**, 3078-3088.
4. X. Y. Lang, A. Hirata, T. Fujita and M. W. Chen, *Nat. Nanotechnol.*, 2011, **6**, 232-236.
5. H. Jiang, P. S. Lee and C. Z. Li, *Energy Environ. Sci.*, 2013, **6**, 41-53.
6. Z. J. Fan, J. Yan, T. Wei, L. J. Zhi, G. Q. Ning, T. Y. Li and F. Wei, Adv. Funct. Mater., 2011, **21**, 2366-2375.
7. L. F. Chen, Z. H. Huang, H. W. Liang, W. T. Yao, Z. Y. Yua and S. H. Yu, *Energy Environ. Sci.*, 2013, **6**, 3331-3338.
8. G. P. Wang, L. Zhang and J. J. Zhang, Chem. Soc. Rev., 2012, **41**, 797-828.
9. K. Xie, X. T. Qin, X. Z. Wang, Y. N. Wang, H. S. Tao, Q. Wu, L. J. Yang and Z. Hu, *Adv. Mater.*, 2012, **24**, 347-352.
10. G. H. Yu, L. B. Hu, N. Liu, H. L. Wang, M. Vosgueritchian, Y. Yang, Y. Cui and Z. N. Bao, *Nano Lett*., 2011, **11**, 4438-4442.
11. H. Jiang , J. Ma , C. Z. Li, *Adv. Mater.*, 2012. **24**, 4197-4202.
12. C. Y. Cao, W. Guo, Z. M. Cui, W. G. Song and W. Cai, *J. Mater. Chem.*, 2011, **21**, 3204-3209.
13. H. L. Wang, H. S. Casalongue, Y. Y. Liang and H. J. Dai, *J. Am. Chem. Soc.*, 2010, **132**, 7472-7477.
14. T. Y. Wei, C. H. Chen, H. C. Chien, S. Y. Lu and C. C. Hu, *Adv. Mater.*, 2010, **22**, 347-351.
15. C. C. Xiang, M. Li, M. J.Zhi, A. Manivannan and N. Q. Wu, *J. Power Sources*, 2013, **226**, 65-70.
16. L. Mao, K. Zhang, H. S. O. Chan and J. S. Wu, *J. Mater. Chem.*, 2012. **22**, 1845-1851.
17. X. Du, C. Y. Wang, M. M. Chen, Y. Jiao and J. Wang, *J. Phys. Chem. C*, 2009, **113**, 2643-2646.
18. W. H. Shi, J. X. Zhu, D. H. Sim, Y. Y. Tay, Z. Y. Lu, X. J. Zhang, Y. Sharma, M. Srinivasan, H. Zhang, H. H. Hng and Q.Y. Yan. *J. Mater. Chem.*, 2011, **21**, 3422-3427.
19. L. Wang, H. M. Ji, S. S. Wang, L. J. Kong, X. F. Jiang and G. Yang, *Nanoscale*, 2013, **5**, 3793-3799.
20. A. B. Deshmukh and M. V. Shelke, *RSC Adv.*, 2013, **3**, 21390-21393.
21. Y. H. Kim and S. J. Park, *Curr. Appl. Phys.*, 2011, **11**,462-466.
22. Q. T. Qu, S. B. Yang and X. L. Feng, *Adv. Mater.*, 2011, **23**, 5574-5580.
23. J. P. Cheng, Q. L. Shou, J. S. Wu, F. Liu, V. P. Dravid and X. B. Zhang, *J. Electroanal. Chem.*, 2013, **698**, 1-8.
24. Q. H. Wang, L. F. Jiao, H. M. Du, Y. J. Wang and H. T. Yuan, *J. Power Sources*, 2014, **245**, 101-106.
25. W. S. Hummers and R. E. Offeman, *J. Am. Chem. Soc.*,1958, **80**, 1339.
26. Z. Gao, J. Wang, Z. Li, W. Yang, B. Wang, M. Hou, Y. He, Q. Liu,T. Mann, P. Yang, M. Zhang and L. Liu, *Chem. Mater.*, 2011, **23**, 3509-3516.
27. J. Chang, H. Xu and J. Sun, *J. Mater. Chem.*, 2012, **22**, 11146-11150.
28. X. L. Yang, K. C. Fan, Y. H. Zhu, J. H. Shen, X. Jiang, P. Zhao and C. Z. Li, *J. Mater. Chem.*, 2012, **22**, 17278-17283.
29. G. M. Zhou, D. W. Wang, F. Li, L. L. Zhang, N. Li, Z. S. Wu, L. Wen, G. Q. Lu and H. M. Cheng, *Chem. Mater.*, 2010, **22**, 5306-5313.
30. F. Zhang, T. F. Zhang, X. Yang, L. Zhang, K. Leng, Y. Huang and Y. S. Chen, *Energy Environ. Sci.*, 2013, **6**, 1623-1632.
31. R. H. Wang, C.H. Xu, J. Sun, L. Gao and C. C. Lin, *J. Mater. Chem. A,* 2013, **1**, 1794-1800.
32. J. Su, M. H. Cao, L. Ren and C. W. Hu, *J. Phys. Chem. C*, 2011, **115**, 14469-14477.
33. X. J. Zhang, W. H. Shi. J. X. Zhu, W. Y. Zhao, J. Ma, S. Mhaisalkar, T. L. Maria, Y. H. Yang, H. Zhang, H. H. Hng and Q. Y. Yan, *Nano Res.*, 2010, **3**, 643-652.
34. P. Simon and Y. Gogotsi, *Nat. Mater.*, 2008, **7**, 845–854.